ARTICLE IN PRESS

Ceramics International xxx (xxxx) xxx

Contents lists available at ScienceDirect

Ceramics International

journal homepage: www.elsevier.com/locate/ceramint

Degradation of residual pharmaceuticals through an accelerated oxidation process using deep ultraviolet (DUV) light and a TiO_2/BDD composite electrode

Kai Takagi [a,b], Norihiro Suzuki [c,*], Izumi Serizawa [b], Yuvaraj M. Hunge [d], Tomonori Suzuki [d], Ken-ichi Katsumata [d], Chiaki Terashima [a,d], Akira Fujishima [d]

[a] *Graduate School of Science and Technology, Tokyo University of Science, 2641 Yamazaki, Noda, Chiba, 278-8510, Japan*
[b] *ORC Manufacturing co., Ltd., 4896 Tamagawa, Chino, Nagano, 391-0011, Japan*
[c] *Department of Natural Sciences, School of Engineering, Tokyo Denki University, 5 Senjyu Asahi-cho, Adachi-ku, Tokyo, 120-8551, Japan*
[d] *Research Institute for Science and Technology, Tokyo University of Science, 2641 Yamazaki, Noda, Chiba, 278-8510, Japan*

ARTICLE INFO

Handling Editor: Dr P. Vincenzini

Keywords:
Titanium dioxide
Boron-doped diamond
Deep ultraviolet light
Residual pharmaceuticals
Accelerated oxidation process
Sulfamethoxazole

ABSTRACT

This study investigates the degradation of sulfamethoxazole (SMX), a persistent pharmaceutical contaminant, using a TiO_2/BDD composite electrode combined with deep ultraviolet (DUV) light and electrolysis. The increasing presence of pharmaceutical residues in water poses environmental and health risks due to their chemical stability and resistance to conventional treatment. Advanced oxidation process (AOP) employs highly reactive species such as hydroxyl radicals and ozone to degrade contaminants, but improving efficiency and electrode stability remains challenging. To address these issues, a TiO_2/BDD composite electrode was prepared via reactive sputtering, enabling simultaneous electrochemical oxidation and photocatalysis while maintaining strong adhesion. The experimental setup evaluated SMX degradation under four conditions: DUV light alone, electrolysis alone, the TiO_2/BDD composite electrode with DUV light, and a fully integrated system combining all three components. Structural characterization confirmed the formation of a stable p-n heterojunction between TiO_2 and BDD, enhancing charge separation and photocatalytic activity. Results showed that the integrated AOP system significantly improved SMX degradation, achieving a 50 % total organic carbon (TOC) removal rate, outperforming electrolysis alone. Raman spectroscopy indicated that oxidation of the TiO_2 film contributed to the formation of highly crystalline anatase, enhancing long-term photocatalytic performance. Additionally, the TiO_2 layer remained intact without delamination, demonstrating durability under reaction conditions. This study highlights the potential of TiO_2/BDD composite electrodes as an efficient, scalable solution for pharmaceutical wastewater treatment, addressing environmental concerns associated with residual pharmaceuticals in aquatic systems.

1. Introduction

The increasing presence of pharmaceutical residues in aquatic environments presents a significant threat to both aquatic and terrestrial organisms, making it a pressing global concern that requires immediate attention [1,2]. Pharmaceuticals play a crucial role in modern medicine due to their extensive applications and beneficial effects in both human and animal healthcare. Among the various residual pharmaceuticals detected in the environment, sulfonamides, which are widely utilized as antibiotics in both human and veterinary medicine, have been frequently identified in surface water and groundwater [3]. In particular, sulfamethoxazole (SMX), a commonly prescribed sulfonamide antibiotic, is one of the most frequently detected pharmaceutical contaminants in water sources [4]. Conventional wastewater treatment processes have proven largely ineffective in removing these pharmaceutical residues, leading to their continuous discharge into the aquatic environment, where they persist and accumulate over extended periods of time [5]. This persistence is primarily due to their inherent chemical stability and strong resistance to biodegradation, enabling them to remain in the environment for prolonged durations [6]. Furthermore,

---

* Corresponding author.
E-mail address: suzuki.norihiro@mail.dendai.ac.jp (N. Suzuki).

https://doi.org/10.1016/j.ceramint.2025.07.107
Received 2 June 2025; Received in revised form 7 July 2025; Accepted 8 July 2025

Please cite this article as: Kai Takagi et al., *Ceramics International*, https://doi.org/10.1016/j.ceramint.2025.07.107

there is increasing concern that these residual pharmaceuticals may be bioaccumulated and biomagnified within aquatic and terrestrial food chains, potentially leading to adverse health effects in humans who consume contaminated water or food. By concerning the environmental and public health risks, it is imperative to advance research efforts aimed at developing and implementing effective methods for the degradation and removal of residual pharmaceuticals from wastewater systems.

In recent years, advanced oxidation process (AOP) have gained significant attention for the degradation of residual pharmaceuticals and persistent organic pollutants in wastewater [7,8]. AOP utilize highly reactive species, such as hydroxyl radicals (•OH), ozone (O_3), and hydrogen peroxide (H_2O_2), to oxidize and decompose these organic contaminants. Through AOP, organic compounds undergo oxidation, converting carbon and oxygen atoms in their molecular structures into carbon dioxide and water, respectively. AOP is considered a safe and environmentally friendly treatment method, as they effectively detoxify contaminants while minimizing the formation of intermediate byproducts. Common AOP primarily employ O_3, H_2O_2, and ultraviolet (UV) light [9]. UV light not only directly cleaves the chemical bonds of residual pharmaceuticals but also facilitates the in situ generation of O_3 and H_2O_2 from water. Deep ultraviolet (DUV) light, with wavelengths ranging from 200 to 300 nm and photon energies between 4.1 and 6.2 eV, is particularly effective at breaking the chemical bonds of a wide range of substances [10]. However, UV light alone generates only limited amounts of O_3, the key oxidant in AOP, resulting in low decomposition efficiency. Additionally, previous studies have reported that UV irradiation can lead to the formation of optical isomers [11].

To enhance the efficiency of advanced oxidation process (AOP), ozone (O_3) generation and photocatalysis are often combined together. In the case of O_3, water electrolysis is used to directly generate O_3 from solution. Boron-doped diamond (BDD) and tin oxide (SnO_2) are commonly employed as electrode materials, with BDD offering superior chemical resistance and durability due to its diamond crystal structure as compared to SnO_2 [12,13]. Photocatalysts, typically composed of titanium oxide (TiO_2), are widely used due to their affordability, chemical stability, and durability [14]. While AOP alone are often inefficient, integrating multiple oxidation mechanisms significantly enhances the oxidation and thereby the degradation of contaminants. However, a key challenge is that these methods are typically implemented separately within treatment systems, leading to increased equipment complexity and bulkiness. Therefore, the development of compact and integrated systems that efficiently combine these approaches is essential.

In our previous study, we successfully achieved complete decomposition of SMX using AOP that integrate three mechanisms electrical, optical, and photocatalytic by employing mesoporous TiO_2/BDD (MP-TiO_2/BDD) and DUV ray lamp. However, this approach is unsuitable for electrode applications due to the low adhesion strength of MP-TiO_2 in MP-TiO_2/BDD, necessitating the use of an additional BDD electrode for O_3 generation [15].

In this study, we prepared a TiO_2/BDD composite electrode by depositing TiO_2 onto BDD via reactive sputtering. Typically, metal oxide layers are prone to delamination due to bubble formation on the electrode surface. To address this issue, we patterned the TiO_2 to expose the underlying BDD, enabling O_3 generation at the BDD regions while facilitating photocatalytic reactions at the TiO_2 regions. This design allows the composite electrode to function simultaneously as an electrode and a photocatalyst. Unlike conventional MP-TiO_2/BDD electrodes that suffer from poor adhesion and structural instability during electrochemical operation, the present electrode demonstrates improved adhesion strength, electrochemical durability, and integrated functionality within a compact system. This work not only advances the electrode design for pharmaceutical degradation but also contributes to the understanding of surface and interface engineering by showing that controlled micro-patterning can enhance both the mechanical stability and photocatalytic performance of p–n heterojunctions. Such improvements are critical for the development of scalable and long-term AOP systems. Finally, we applied various methods to decompose SMX and evaluated the durability of the composite electrode, confirming that the patterned TiO_2 remained intact without delamination.

2. Experimental

2.1. Materials and chemicals

All chemicals and materials used in the fabrication of the TiO_2/BDD composite electrode and the SMX degradation experiments were used as received without further purification. The TiO_2/BDD composite electrode was prepared using a single-crystal silicon substrate (Si, 111, Nilaco), a titanium metal target (Ti, 99.5 %, Nilaco), diamond powder (MICRON + CDA™, Element Six), acetone (C_3H_6O, 99.8 %, Wako), methanol (CH_3OH, 99.8 %, Wako), boron oxide (B_2O_3, 95.0 %, Kanto Chemical), sulfuric acid (H_2SO_4, 95.0 %, Wako), positive photoresist (THMR-iP5700HP, Tokyo Ohka Kogyo), and resist stripper (TMAH 2.38 %, Tokyo Ohka Kogyo). O_2, Ar, and H_2 (99.99995 vol%, Taiyo Nippon Sanso) were used as process gases during deposition. For comparison, the MP-TiO_2/BDD electrode was synthesized using a diblock copolymer (PS(18000)-*b*-PEO(7500), Polymer Source), titanium chloride ($TiCl_4$, 99.0 %, Wako), concentrated hydrochloric acid (HCl, 37 wt%, Wako), tetrahydrofuran (THF, 99.5 %, Wako), and ethanol (C_2H_5OH, 99.5 %, Wako). The SMX degradation experiments utilized a platinum mesh (#80, 99.95 %, Nilaco), a proton exchange membrane (Nafion™ NRE-212, Sigma-Aldrich), UV-curing sealant (3035B, Three Bond), conductive silver paste (D-550, Fujikura Kasei), Teflon-coated copper wire (φ1.0 mm, Nilaco), phosphate buffer powder (pH 7.0, Wako), and sulfamethoxazole (SMX, 98.0 %, Wako). All solutions were prepared using deionized water with a conductivity of approximately 18 MΩ cm.

2.2. Preparation of TiO_2/BDD composite electrodes

The preparation process of the TiO_2/BDD composite electrode was illustrated in Fig. 1. The deposition of BDD and TiO_2 followed the method developed by Terashima et al. [16]. First, 15 × 15 mm single-crystal silicon substrate was mechanically seeded with diamond powder by rubbing for 20 min. The substrate was then ultrasonically cleaned in acetone, methanol, and deionized water for 10 min each. BDD film deposition was performed using a microwave plasma chemical vapor deposition (MP-CVD) system (AX6500, ASTex) under the following conditions: H_2 flow rate of 500 sccm, chamber pressure of 90 Torr, plenum pressure of 70 Torr, microwave power of 5500 W, and H_2 bubbling gas at 0.5 sccm. The precursor solution consisted of acetone: methanol (9 : 1) with B_2O_3 dissolved to achieve a boron-to-carbon ratio of 10,000 ppm. The deposition was carried out for 4 h. Photoresist layer was then spin-coated onto the BDD surface using a spin coater (MS-A200, MIKASA) at 3000 rpm for 10 s, followed by baking at 90 °C for 90 s. Mask with a 100 μm line/space pattern was placed over the photoresist and exposed to Xe lamp irradiation (UV•7, U-VIX) at 250 mW/cm^2 (at 365 nm) for 1s, followed by baking at 110 °C for 90 s. The uncured photoresist was removed using a resist stripper and deionized water. TiO_2 film deposition was carried out using a high-frequency sputtering system (VTR-150M/SRF, ULVAC) with a Ti target. The deposition conditions were as follows: pressure of 1.0 Pa, Ar and O_2 flow rates of 30 sccm each, RF power of 250 W, and substrate heating at 200 °C for 90 min. Following TiO_2 deposition, the cured resist was removed with acetone, and anodization cleaning was performed in a 0.5 M H_2SO_4 aqueous solution for 10 min at a current of 10 mA. The resulting substrate was used as the TiO_2/BDD composite electrode.

The surface morphology of the prepared TiO_2/BDD composite electrode was analyzed using laser microscope (VK-X200, KEYENCE) and field-emission scanning electron microscopy (FE-SEM, JSM-7600F, JEOL). Elemental mapping of the TiO_2/BDD composite electrode was performed using energy-dispersive X-ray spectroscopy (EDS).

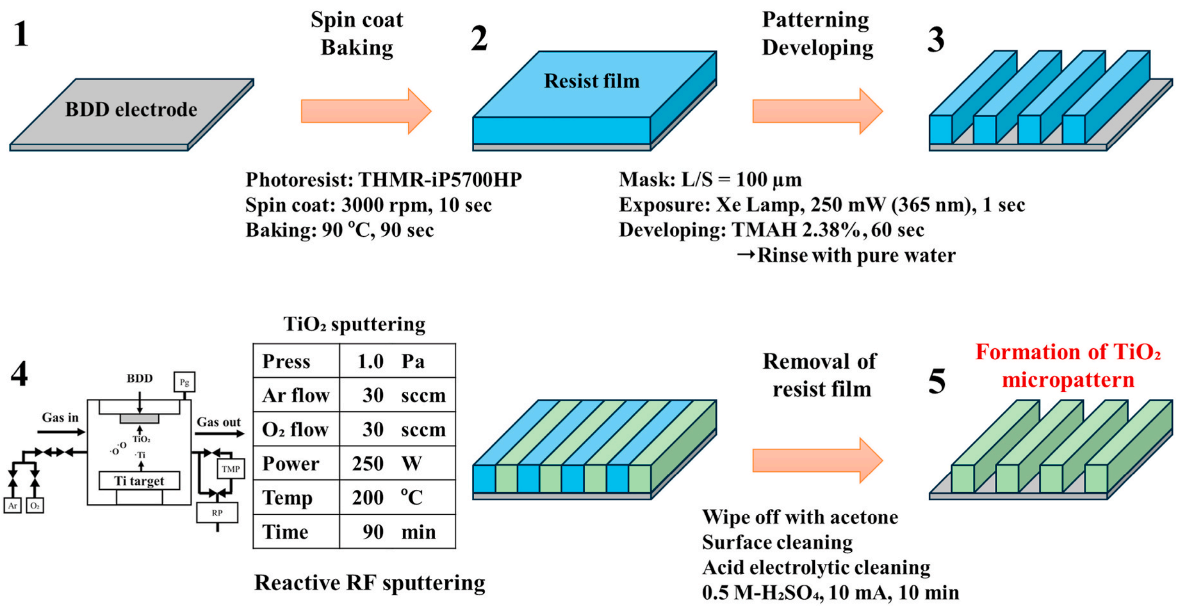

Fig. 1. Preparation process for TiO_2/BDD composite electrode.

Additionally, the BDD and TiO_2 films were characterized using laser Raman microscopy (NRS-5100, JASCO) with a 532 nm excitation wavelength.

The photo-responsiveness of the TiO_2/BDD composite electrode was evaluated using a three-electrode single-cell (Fig. 1S). Working electrode was made by adhering Teflon-coated Cu wire to the single-crystal silicon substrate using conductive silver paste, and coating the back surface and surrounding area with UV-cured resin. The working electrode was positioned 2 mm from a quartz tube containing DUV light lamp (excimer UV lamp, 222 nm, ORC Manufacturing). Reference electrode, counter electrode, and electrolyte were Ag/AgCl (RE-1B, BAS), platinum mesh (#80, 99.5 %, Nilaco, 15 × 15 mm), and 0.5 M-Na_2SO_4 aqueous solution, respectively. The illuminance of the DUV light lamp was measured using laser power/energy meter (VEGA, OPHIR) and was determined to be 1.2 mW/cm^2 (at 222 nm) at the tube wall. Prior to photo-response measurements, the solution was purged with N_2 for 30 min to remove dissolved oxygen. Chronoamperometry was performed using potentio/galvanostat (VersaSTAT 4, AMETEK) at a constant potential of 0 V (vs. Ag/AgCl). Once the current stabilized, the DUV light lamp was switched on and off at 20 s intervals to assess the electrode's photo-response.

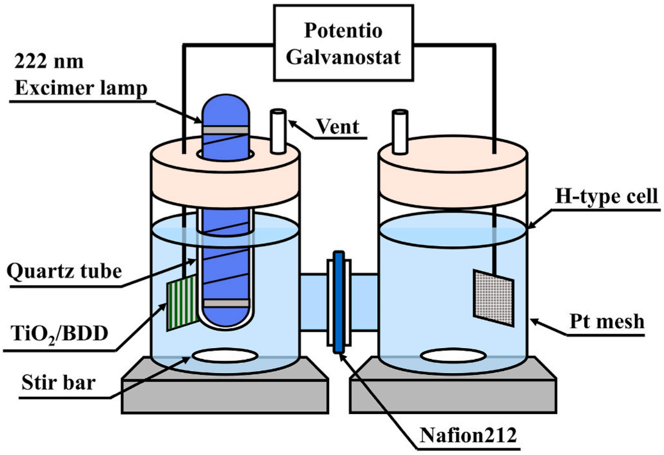

Fig. 2. Schematic diagram of SMX decomposition using DUV light lamp and TiO_2/BDD composite electrode.

2.3. *Decomposition of residual pharmaceuticals*

A schematic diagram of the SMX decomposition experiment is shown in Fig. 2. TiO_2/BDD composite electrode and platinum mesh were used as working and counter electrodes, respectively, in an H-type cell. Proton exchange membrane was used to separate the solution compartments. As in the photo-response evaluation, the working electrode was positioned 2 mm from quartz tube containing a deep DUV light lamp. Electrolyte solution in both compartment (working and counter electrodes) was a 0.25 M-phosphate buffer solution, with 50 ppm SMX dissolved only in working electrode compartment. The solution was continuously stirred throughout the experiment. SMX degradation was examined under four conditions based on the configurations shown in Fig. 2. The patterns were as follows: 1. DUV light lamp only (DUV), 2. Electrolysis using only the TiO_2/BDD composite electrode (Electrolysis), 3. DUV light lamp + TiO_2/BDD composite electrode (DUV + TiO_2/BDD), 4. DUV light lamp + TiO_2/BDD composite electrode + electrolysis (DUV + TiO_2/BDD + Electrolysis). Electrolysis was performed using a potentiostat/galvanostat (HABF5001, MEIDEN HOKUTO) equipped with a power booster (HABF5001-B10, MEIDEN HOKUTO), maintaining a constant current of 75 mA. SMX concentrations were measured at 90 and 180 min using high-performance liquid chromatography (HPLC, LC-2010, Shimadzu) with a Waters Xterra MS C18 column. The HPLC detector was set at wavelength of 270 nm, the column temperature was maintained at 25 °C, and the mobile phase consisted of a 0.25 M -acetic acid: acetonitrile solution (7:3) at a flow rate of 0.5 mL/min. After 180 min of SMX degradation, total organic carbon (TOC) concentrations were analyzed using a TOC analyzer (TOC-V_{CSH}, Shimadzu). MP-TiO_2/BDD was prepared using the procedure reported previously for comparison [17]. As shown in Fig. S2, MP-TiO_2/BDD had a mesoporous structure with a pore size of approximately 20 nm. MP-TiO_2/BDD was evaluated under the same conditions as the DUV + MP-TiO_2/BDD + Electrolysis configuration. The evaluation of MP-TiO_2/BDD was based solely on TOC concentration. Since the MP-TiO_2 film on the BDD delaminated immediately during electrolysis, a new BDD electrode was installed and used as shown in Fig. S3.

3. Results and discussion

3.1. Morphological and structural characterizations

Laser microscopic images illustrating each step of the TiO_2/BDD composite electrode preparation process, along with an SEM image and elemental mapping of the TiO_2/BDD electrode, are shown in Fig. 3. Following BDD film deposition, crystalline structures with random particle sizes of up to 5 μm were observed on the single-crystal silicon substrate [18]. The crystals exhibited an irregular polycrystalline morphology. After photoresist patterning, lines with widths of 85 μm and 115 μm were formed in the photoresist and BDD layers, respectively, with a photoresist thickness of 2.00 μm. The mask was designed with a line/space pattern of 100 μm; however, the actual photoresist width was slightly narrower than intended. This discrepancy is likely due to overexposure caused by incomplete parallel light irradiation. Minute gaps between the photoresist and the mask may have allowed light leakage, further affecting the pattern dimensions. Following TiO_2 film deposition, a green film was observed in the regions where the photoresist lines were absent. It has been reported that titanium can produce various colors when oxidized, suggesting that a titanium oxide film was formed. [19]. The film exhibited a width of 115 μm and a thickness of 0.40 μm. SEM imaging and elemental mapping confirmed the presence of Ti and O in the green film, with Ti and O content ratios of 37.5 % and 62.5 %, respectively. Cross-sectional SEM analysis (Fig. S4) revealed a TiO_2 film thickness of 0.38 μm, consistent with the laser microscopy measurements. The BDD layer had a thickness of 6 μm on the Si substrate. A small gap was observed between the TiO_2 film and the BDD layer, likely caused by delamination during sample preparation. This inference is supported by the absence of a gap on the left side of the cross-sectional SEM image.

Fig. 4 presents the Raman spectra of BDD, the TiO_2/BDD composite electrode after TiO_2 film deposition, after anodization, and ST-01. ST-01 consists of more than 99 % anatase phase. The spectral intensity of all samples, except for ST-01, was relatively weak and was therefore amplified by a factor of 20 for clarity. The Raman spectrum of ST-01 exhibited characteristic anatase peaks, including three symmetric stretching vibration (E_g) peaks at 144, 194, and 639 cm^{-1}, two lattice rotational vibration (B_{1g}) peaks at 397 and 517 cm^{-1}, and one stretching vibration (A_{1g}) peak at 517 cm^{-1} [20,21]. The B_{1g} and A_{1g} peaks near 517 cm^{-1} overlap, as their peak positions are nearly identical. In the BDD film, peaks corresponding to the maximum values of the phonon density of states (PDOS), boron dimers and clustered boron (B-B), and zone-center phonon states (ZCP) were observed at 497, 1228, and 1322 cm^{-1}, respectively [22-24]. Before anodization, the Raman spectrum of the TiO_2/BDD composite electrode exhibited a small peak attributed to the anatase phase. Reactive RF sputtering enables low-temperature film deposition. TiO_2 predominantly forms the anatase phase at lower temperatures and transitions to the rutile phase at higher temperatures. Consequently, the TiO_2/BDD composite electrode contained anatase, which is known for its high photocatalytic activity [25,26]. After anodization, the intensity of the anatase-related peak increased. Previous studies have reported that anodization promotes the formation of both anatase and rutile phases in titanium-based materials [27,28]. Therefore, it is likely that the anatase phase in the TiO_2/BDD composite

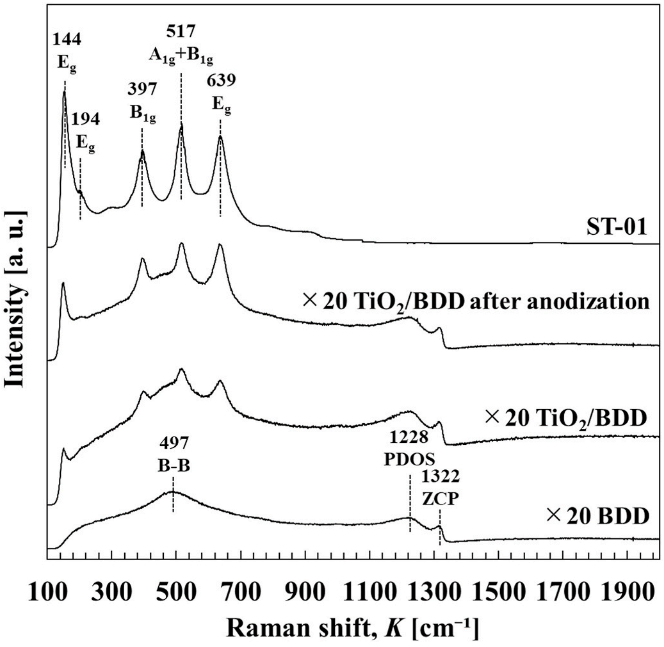

Fig. 4. Raman spectra of ST-01, BDD, TiO_2/BDD and TiO_2/BDD after anodization.

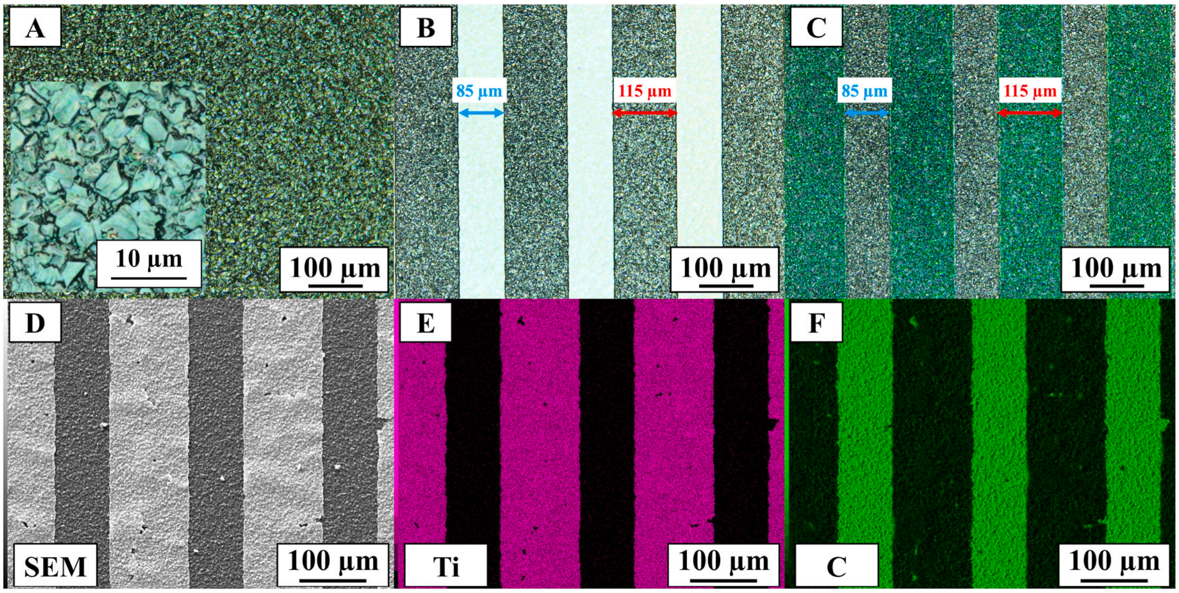

Fig. 3. Laser microscope images of BDD (A), after patterning (B), and after TiO_2 patterning (C) and SEM image (D) and elemental maps (E, F) of the TiO_2/BDD composite electrode.

electrode underwent further crystallization and growth during the anodization process.

The photo-response of BDD and TiO_2/BDD under on-off switching of the DUV light lamp is shown in Fig. 5. The BDD electrode exhibited a photocurrent of approximately −5 μA. When doped with boron, BDD behaves as a p-type semiconductor with a bandgap of approximately 5.1 eV [29,30]. DUV light at wavelength of 222 nm corresponds to an energy of 5.6 eV, which is sufficient to excite BDD, leading to electron emission into the solution [31]. In contrast, TiO_2/BDD composite electrode exhibited a photocurrent of approximately 20 μA. This increase is attributed to the heterojunction formation between the n-type TiO_2 and p-type BDD, where hole accumulation in the TiO_2 layer resulted in a positive photocurrent response [32]. While bare BDD without a TiO_2 layer is expected to exhibit photoactivity, the absence of a detectable photo-response suggests that surface termination influences electron transfer [33]. Anodization likely led to oxygen termination of the BDD surface, which suppressed photoexcitation under light exposure. This modification may have altered the electronic properties of BDD, preventing significant charge carrier generation.

3.2. Decomposition of residual pharmaceuticals

The chromatograms of the solution after 90 min in SMX decomposition experiments using each method, as well as the time-dependent changes in SMX concentration, are shown in Figs. 6 and 7, respectively. In the blank sample (before SMX degradation), a prominent peak corresponding to SMX was detected at 12.5 min, along with a smaller peak at 4.5 min, attributed to electrolyte components. During electrolysis, bubble formation was observed exclusively on the BDD surface of the TiO_2/BDD composite electrode. After 90 min of electrolysis, a significant SMX peak remained, indicating limited degradation. In contrast, in all other treatment methods, the SMX peak disappeared, suggesting complete or near-complete degradation. In HPLC analysis, compounds with lower molecular weights typically exhibit shorter retention times. Additionally, the C18 reverse-phase column used in this study retains more hydrophobic compounds for longer durations. Based on these principles, it is inferred that AOP oxidized SMX into lower-molecular-weight, more hydrophilic compounds, likely containing functional groups such as hydroxyl (-OH) and nitro ($-NO_2$) groups. Various intermediate products may form during SMX degradation; however, their identification has already been reported in previous studies [15]. Based on the detector settings at 270 nm, the detectable substances likely include aromatic compounds, conjugated systems, and other organic molecules with significant UV absorption at this wavelength. In contrast, electrolysis alone led to a 70 % reduction in SMX concentration over 180 min, bringing it down to 15 mg/L. The primary oxidants in electrolysis, O_3 (ozone) and •OH (hydroxyl radicals), exhibit high oxidation capacity, contributing to the degradation process [34,35]. BDD can generate O_3 (ozone) and •OH (hydroxyl radicals) with high efficiency due to its wide potential window and superior chemical stability compared to SnO_2 and PbO_2 [36]. However, the efficiency of O_3 (ozone)

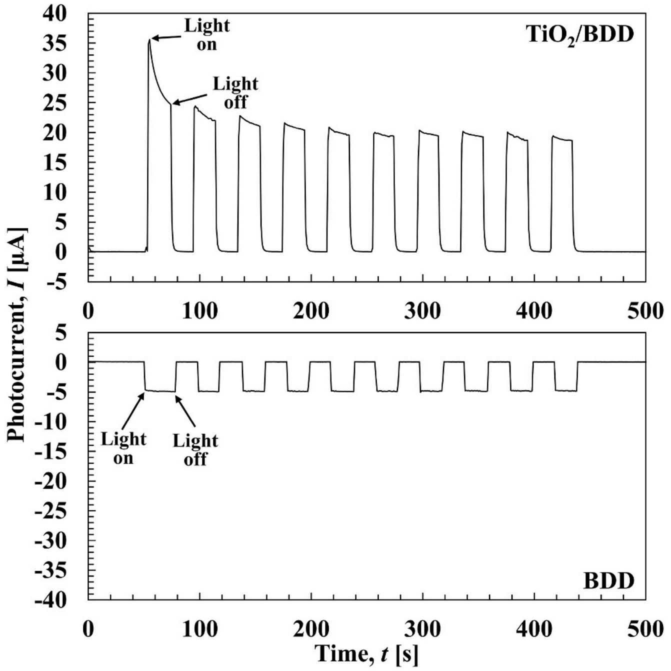

Fig. 5. The photo-response of BDD and TiO_2/BDD under on-off switching of DUV light lamp.

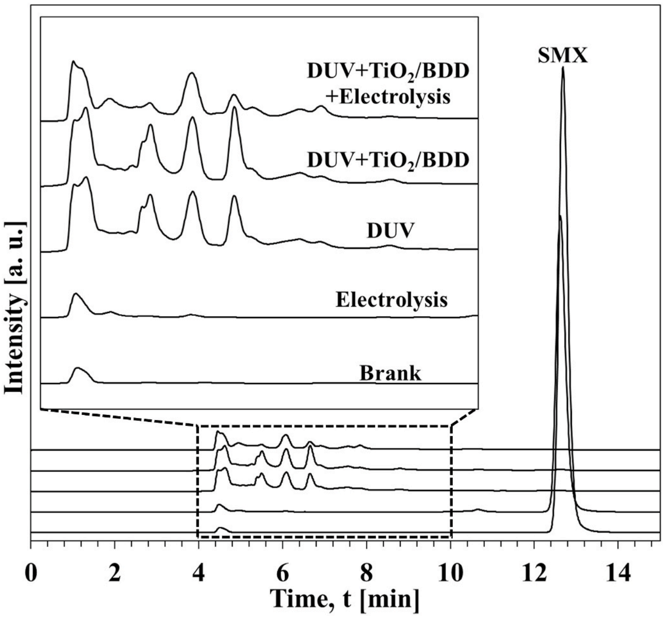

Fig. 6. Chromatograms of solution after 90 min in SMX decomposition experiments using each method.

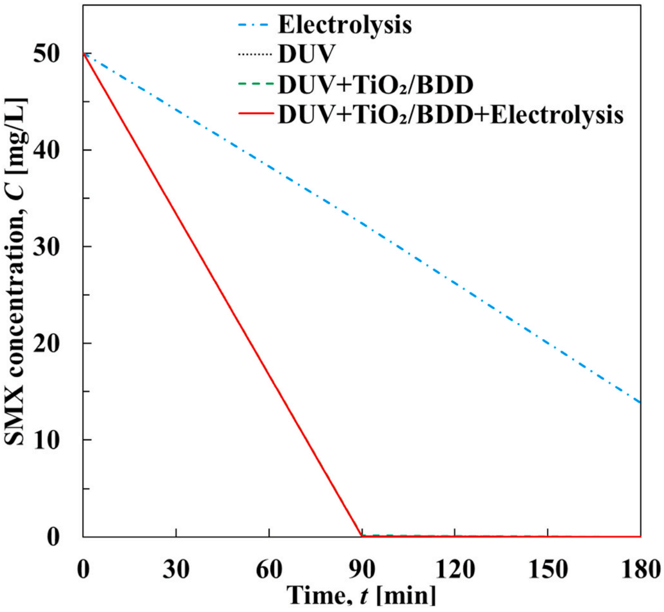

Fig. 7. Time dependence of SMX concentration in SMX decomposition experiments using each method.

and •OH (hydroxyl radical) production is low for untreated plate-form BDD due to its large surface crystal size and small specific surface area [37]. Therefore, the decrease in the SMX removal rate during electrolysis is likely due to the limited efficiency of O_3 and •OH generation. Additionally, the slower degradation rate observed in electrolysis suggests that O_3 alone is less effective for SMX degradation compared to AOP incorporating H_2O_2, where synergistic oxidation enhances overall efficiency.

Fig. 8 presents the TOC removal rates in SMX decomposition experiments using various methods. The TOC removal rate was calculated by dividing the TOC concentration obtained from the TOC analyzer by the initial carbon concentration (23.7 mg/L), which corresponds to 50 mg/L SMX. In the electrolysis, DUV, and DUV + TiO_2/BDD processes, the TOC removal rate remained below 10 %, indicating that most intermediate SMX degradation products persisted in the solution. While SMX degraded rapidly due to the absence of pre-existing intermediates, its decomposition primarily resulted in the formation of stable byproducts, leading to minimal TOC removal. In contrast, the DUV + TiO_2/BDD + Electrolysis method significantly improved the TOC removal rate to 50 %. The integration of all three oxidation mechanisms demonstrated strong oxidative capabilities, effectively breaking down intermediate products despite their high abundance. The DUV + MP-TiO_2/BDD + Electrolysis method, used for comparison, achieved a TOC removal rate exceeding 95 %. However, as described in the experimental section, the MP-TiO_2 layer delaminated almost immediately upon electrolysis, with peeling observed across the entire BDD surface. While MP-TiO_2 membranes enhance AOP efficiency, their instability remains a challenge for system miniaturization. Suzuki et al. [15] achieved almost complete SMX degradation and TOC reduction to below 0.5 mg/L after 8 h using a MP-TiO_2/BDD photocatalyst and a separate BDD electrode under DUV irradiation (222 nm, 1.2 mW/cm^2) and electrochemical oxidation at 75 mA. However, their system suffered from significant delamination of the TiO_2 layer during electrochemical operation. In this study, using the same DUV conditions and current, SMX degradation with the TiO_2/BDD composite electrode reached approximately 50 % TOC removal after 3 h without any electrode delamination. While the degree of mineralization was lower, our sputtered single-electrode design offers superior mechanical stability and simpler system configuration, making it more practical for long-term use. Zeng et al. [38], synthesized a reduced TiO_2 nanotube arrays-based titanium membrane (RTNA/TM) was fabricated by a facile electrochemical method and studied the electrochemical oxidation of sulfamethoxazole (SMX) with the removal rate of 86.1 % and electrical efficiency per order of 0.55 kWh/m^3. Zhang et al. [39], prepared $TiO_2@Fe_2O_3@g\text{-}C_3N_4$ (MFTC) photocatalyst using molecularly imprinted method and studied the photocatalytic degradation of sulfamethoxazole (SMX) degradation under the solar light illumination and found that 96.8 % degradation efficiency.

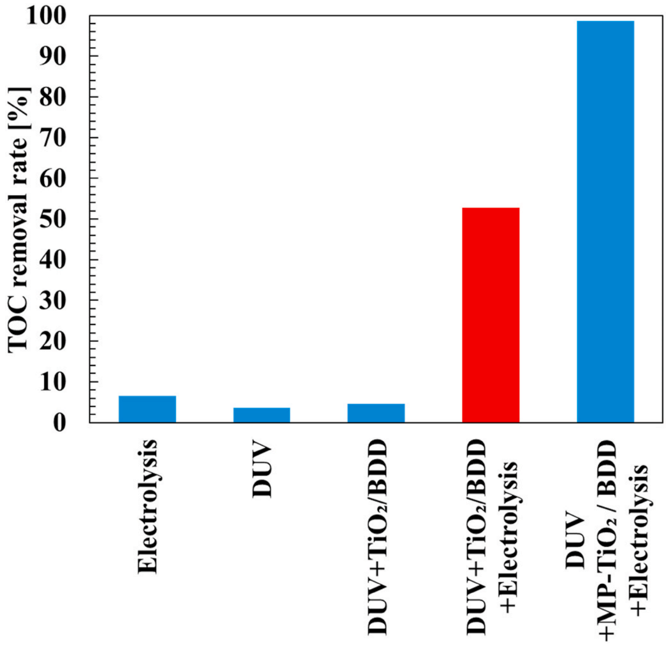

Fig. 8. TOC removal rates in SMX decomposition experiments using each method.

After SMX decomposition, no significant delamination of the TiO_2/BDD composite electrode was observed, indicating that the TiO_2 layer exhibited sufficient adhesion strength to withstand electrolysis without peeling. Notably, some regions of the TiO_2 layer changed from green to a mottled white and pink appearance (Fig. 9A). Raman microscopy analysis of the white areas confirmed the presence of highly crystalline anatase phases with high purity (Fig. 9B). Based on the SMX decomposition experiment, it is inferred that oxidation of the TiO_2 film occurred during the reaction, leading to the formation and growth of trace amounts of anatase [40]. These findings suggest that the TiO_2/BDD composite electrode may undergo gradual structural modifications, enhancing its photocatalytic activity over time and potentially leading to long-term performance improvements.

The functions of the TiO_2/BDD composite electrodes developed in this study are as follows: On the BDD surface, O_3 is electrochemically generated. At this stage, even under DUV light irradiation, photoexcitation does not occur, as the surface is sufficiently oxidized. Upon DUV light irradiation, both the TiO_2 layer and BDD undergo excitation, leading to hole generation. The formation of a p-n heterojunction allows electrons excited in the TiO_2 layer to be captured by holes in BDD, thereby enhancing photocatalytic activity. The high-purity anatase phase is stabilized by the surrounding low-crystallinity TiO_2 layer, ensuring structural integrity. This arrangement ensures that even with bubble formation on the BDD surface, the low-adhesion anatase phase remains intact, contributing to the high durability of the electrode. This structural and functional synergy reinforces the electrode's efficiency and stability for long-term applications.

However, it should be noted that the present study was conducted using a model solution containing SMX in a controlled phosphate buffer. In actual wastewater, the presence of diverse organic and inorganic species, surfactants, and potential fouling agents may significantly impact the degradation efficiency and electrode stability [34,35]. These matrix effects must be considered when extrapolating the current findings to practical applications. Additionally, while the TiO_2/BDD composite electrode maintained its structural integrity throughout a single degradation cycle, its long-term operational stability, resistance to fouling, and performance under continuous flow conditions remain unverified. Furthermore, this study did not investigate the formation and toxicity of intermediate degradation byproducts in detail. Future work should include comprehensive byproduct analysis using advanced techniques such as LC–MS to ensure environmental safety and complete mineralization. This omission limits the ability to assess the environmental safety of the treated water and the completeness of mineralization. Therefore, while the results demonstrate promising catalytic performance, they should be interpreted within the context of these experimental constraints.

4. Conclusions

This study successfully developed a TiO_2/BDD composite electrode via reactive sputtering for the efficient degradation of residual pharmaceuticals, specifically SMX. By integrating DUV light irradiation, electrolysis, and photocatalysis, a highly effective AOP was achieved. The TiO_2/BDD composite electrode demonstrated significant advantages over the conventional MP-TiO_2/BDD by maintaining structural integrity and ensuring high durability during electrolysis. Experimental results showed that the combination of DUV light, TiO_2/BDD

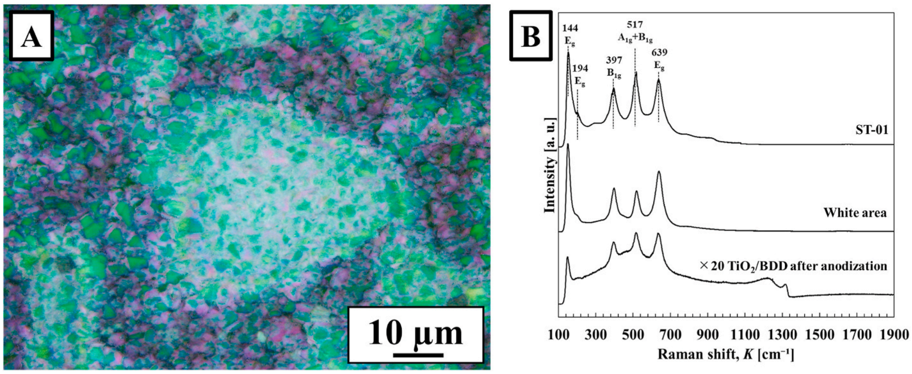

Fig. 9. Laser microscope image of TiO_2/BDD surface after SMX decomposition experiment (A) and Raman spectrum of white area (B).

photocatalysis, and electrochemical oxidation synergistically enhanced SMX degradation and TOC removal. While electrolysis alone resulted in limited SMX decomposition, the integrated AOP system exhibited superior efficiency, achieving a 50 % TOC removal rate. Additionally, the TiO_2/BDD composite electrode exhibited excellent adhesion properties, preventing delamination—a key issue observed in MP-TiO_2/BDD. Structural and photoelectrochemical analyses confirmed the formation of a p-n heterojunction between TiO_2 and BDD, leading to enhanced photocatalytic activity. Furthermore, Raman spectroscopy indicated that the oxidation of the TiO_2 film during electrolysis contributed to the formation of highly crystalline anatase, potentially improving long-term photocatalytic performance. Overall, this study highlights the potential of the TiO_2/BDD composite electrode as a durable and efficient solution for pharmaceutical wastewater treatment. The findings pave the way for the development of compact and scalable AOP systems capable of addressing the environmental challenges posed by pharmaceutical contaminants in water sources.

CRediT authorship contribution statement

Kai Takagi: Writing – original draft, Methodology, Data curation, Conceptualization. **Norihiro Suzuki:** Writing – original draft, Methodology, Data curation, Conceptualization. **Izumi Serizawa:** Funding acquisition. **Yuvaraj M. Hunge:** Writing – review & editing. **Tomonori Suzuki:** Formal analysis. **Ken-ichi Katsumata:** Formal analysis. **Chiaki Terashima:** Project administration, Funding acquisition. **Akira Fujishima:** Supervision.

Declaration of competing interest

The authors declare that they have no known competing financial interests or personal relationships that could have appeared to influence the work reported in this paper.

Acknowledgements

The study was financially supported by the Joint Usage/Research Program of the Tokyo University of Science Photocatalysis International Research Center, Research Institute for Science and Technology, Japan.

Appendix A. Supplementary data

Supplementary data to this article can be found online at https://doi.org/10.1016/j.ceramint.2025.07.107.

References

[1] W. Li, Occurrence, sources, and fate of pharmaceuticals in aquatic environment and soil, Environ. Pollut. 187 (2014) 193–201, https://doi.org/10.1016/j.envpol.2014.01.015.

[2] D. Fatta-Kassinos, S. Meric, A. Nikolaou, Pharmaceutical residues in environmental waters and wastewater: current state of knowledge and future research, Anal. Bioanal. Chem. 399 (1) (2011) 251–275, https://doi.org/10.1007/s00216-010-4300-9.

[3] S. Mohring, I. Strzysch, M. Fernandes, T. Kiffmeyer, J. Tuerk, G. Hamscher, Degradation and elimination of various sulfonamides during anaerobic fermentation: a promising step on the way to sustainable pharmacy? Environ. Sci. Technol. 43 (7) (2009) 2569–2574, https://doi.org/10.1021/es802042d.

[4] G. Prasannamedha, P. Kumar, A review on contamination and removal of sulfamethoxazole from aqueous solution using cleaner techniques: present and future perspective, J. Clean. Prod. 250 (2020), https://doi.org/10.1016/j.jclepro.2019.119553.

[5] K. Tang, G. Ooi, E. Torresi, K. Kaarsholm, A. Hambly, K. Sundmark, S. Lindholst, C. Sund, C. Kragelund, M. Christensson, K. Bester, H. Andersen, Municipal wastewater treatment targeting pharmaceuticals by a pilot-scale hybrid attached biofilm and activated sludge system (hybas™), Chemosphere 259 (2020), https://doi.org/10.1016/j.chemosphere.2020.127397.

[6] J. Sousa, A. Ribeiro, M. Barbosa, M. Pereira, A. Silva, A review on environmental monitoring of water organic pollutants identified by EU guidelines, J. Hazard Mater. 344 (2018) 146–162, https://doi.org/10.1016/j.jhazmat.2017.09.058.

[7] D. Kanakaraju, B. Glass, M. Oelgemöller, Advanced oxidation process-mediated removal of pharmaceuticals from water: a review, J. Environ. Manag. 219 (2018) 189–207, https://doi.org/10.1016/j.jenvman.2018.04.103.

[8] M. Klavarioti, D. Mantzavinos, D. Kassinos, Removal of residual pharmaceuticals from aqueous systems by advanced oxidation processes, Environ. Int. 35 (2) (2009) 402–417, https://doi.org/10.1016/j.envint.2008.07.009.

[9] R. Andreozzi, V. Caprio, A. Insola, R. Marotta, Advanced oxidation processes (AOP) for water purification and recovery, Catal. Today 53 (1) (1999) 51–59.

[10] Q. Bai, Q. Wu, B. Ye, Y. Wu, J. Lee, M. Lee, W. Wang, Assessing excimer far-UVC (222 nm) irradiation for advanced oxidation processes: oxidants photochemistry and micropollutants degradation, Water Res. 267 (2024), https://doi.org/10.1016/j.watres.2024.122505.

[11] M. Díaz-Cruz, M. Llorca, D. Barceló, Organic UV filters and their photodegradates, metabolites and disinfection by-products in the aquatic environment, Trac. Trends Anal. Chem. 27 (10) (2008) 873–887, https://doi.org/10.1016/j.trac.2008.08.012.

[12] B. Adams, M. Tian, A. Chen, Design and electrochemical study of SnO2-based mixed oxide electrodes, Electrochim. Acta 54 (5) (2009) 1491–1498, https://doi.org/10.1016/j.electacta.2008.09.034.

[13] O. Cornejo, M. Murrieta, L. Castañeda, J. Nava, Characterization of the reaction environment in flow reactors fitted with BDD electrodes for use in electrochemical advanced oxidation processes: a critical review, Electrochim. Acta 331 (2020), https://doi.org/10.1016/j.electacta.2019.135373.

[14] J. Alvarez-Corena, J. Bergendahl, F. Hart, Advanced oxidation of five contaminants in water by UV/TiO2: reaction kinetics and byproducts identification, J. Environ. Manag. 181 (2016) 544–551, https://doi.org/10.1016/j.jenvman.2016.07.015.

[15] N. Suzuki, A. Okazaki, K. Takagi, I. Serizawa, Y. Hirami, H. Noguchi, S. Pitchaimuthu, C. Terashima, T. Suzuki, N. Ishida, K. Nakata, K. Katsumata, T. Kondo, M. Yuasa, A. Fujishima, Complete decomposition of sulfamethoxazole during an advanced oxidation process in a simple water treatment system, Chemosphere 287 (2022), https://doi.org/10.1016/j.chemosphere.2021.132029.

[16] C. Terashima, R. Hishinuma, N. Roy, Y. Sugiyama, S. Latthe, K. Nakata, T. Kondo, M. Yuasa, A. Fujishima, Charge separation in TiO2/BDD heterojunction thin film for enhanced photoelectrochemical performance, ACS Appl. Mater. Interfaces 8 (3) (2016) 1583–1588, https://doi.org/10.1021/acsami.5b10993.

[17] N. Suzuki, A. Okazaki, H. Kuriyama, I. Serizawa, A. Hara, Y. Hirano, Y. Nakabayashi, N. Roy, C. Terashima, K. Nakata, K. Katsumata, T. Kondo, M. Yuasa, A. Fujishima, Synthesis of mesoporous TiO2/Boron-Doped diamond photocatalyst and its photocatalytic activity under deep UV light (=222 nm) irradiation, Molecules 23 (12) (2018), https://doi.org/10.3390/molecules23123095.

[18] D. Gandini, P. Michaud, I. Duo, E. Mahé, W. Haenni, A. Perret, C. Comninellis, Electrochemical behavior of synthetic boron-doped diamond thin film anodes, N. Diamond Front. Carbon Technol. 9 (5) (1999) 303–316.

[19] Y. Tsai, P. Song, J. Fang, Colorful oxide film formation on titanium by using EDM process, Int. J. Precis. Eng. Manuf. 14 (11) (2013) 1933–1937, https://doi.org/10.1007/s12541-013-0262-0.

[20] A. Orendorz, A. Brodyanski, J. Lösch, L. Bai, Z. Chen, Y. Le, C. Ziegler, H. Gnaser, Phase transformation and particle growth in nanocrystalline anatase TiO2 films analyzed by X-ray diffraction and Raman spectroscopy, Surf. Sci. 601 (18) (2007) 4390–4394, https://doi.org/10.1016/j.susc.2007.04.127.

[21] S. El-Deen, A. Hashem, A. Ghany, S. Indris, H. Ehrenberg, A. Mauger, C. Julien, Anatase TiO2 nanoparticles for lithium-ion batteries, Ionics 24 (10) (2018) 2925–2934, https://doi.org/10.1007/s11581-017-2425-y.

[22] M. Bernard, C. Baron, A. Deneuville, About the origin of the low wave number structures of the Raman spectra of heavily boron doped diamond films, Diam. Relat. Mater. 13 (4–8) (2004) 896–899, https://doi.org/10.1016/j.diamond.2003.11.082.

[23] V. Sidorov, E. Ekimov, Superconductivity in diamond, Diam. Relat. Mater. 19 (5–6) (2010) 351–357, https://doi.org/10.1016/j.diamond.2009.12.002.

[24] F. Pruvost, A. Deneuville, Analysis of the Fano in diamond, Diam. Relat. Mater. 10 (3–7) (2001) 531–535.

[25] B. Weinberger, R. Garber, TITANIUM-DIOXIDE photocatalysts produced by reactive magnetron sputtering, Appl. Phys. Lett. 66 (18) (1995) 2409–2411.

[26] D. Rafieian, W. Ogieglo, T. Savenije, R. Lammertink, Controlled formation of anatase and rutile TiO2 thin films by reactive magnetron sputtering, AIP Adv. 5 (9) (2015), https://doi.org/10.1063/1.4931925.

[27] M. Diamanti, M. Pedeferri, Effect of anodic oxidation parameters on the titanium oxides formation, Corros. Sci. 49 (2) (2007) 939–948, https://doi.org/10.1016/j.corsci.2006.04.002.

[28] N. Kuromoto, R. Simao, G. Soares, Titanium oxide films produced on commercially pure titanium by anodic oxidation with different voltages, Mater. Char. 58 (2) (2007) 114–121, https://doi.org/10.1016/j.matchar.2006.03.020.

[29] R. Kalish, Doping of diamond, Carbon 37 (5) (1999) 781–785.

[30] V. Srikanth, P. Kumar, V. Kumar, A brief review on the in situ synthesis of boron-doped diamond thin films, Intern. J. Electrochemistry 2012 (2012), https://doi.org/10.1155/2012/218393.

[31] A. Sakharova, Y. Pleskov, F. Diquarto, S. Piazza, C. Sunseri, I. Teremetskaya, V. Varnin, Synthetic diamond electrodes - photoelectrochemical investigation of undoped and boron-doped polycrystalline thin-films, J. Electrochem. Soc. 142 (8) (1995) 2704–2709.

[32] M. Behul, M. Vojs, M. Marton, P. Michniak, M. Mikolásek, M. Kurniawan, H. Honig, D. Zyabkin, M. Ramirez, L. Spiess, D. Flock, A. Bund, M. Papula, R. Redhammer, Nanostructured boron doped diamond enhancing the photoelectrochemical performance of TiO2/BDD heterojunction anodes, Vacuum 171 (2020), https://doi.org/10.1016/j.vacuum.2019.109006.

[33] T. Rao, D. Tryk, K. Hashimoto, A. Fujishima, Band-edge movements of semiconducting diamond in aqueous electrolyte induced by anodic surface treatment, J. Electrochem. Soc. 146 (2) (1999) 680–684.

[34] E. Brillas, C. Martínez-Huitle, Decontamination of wastewaters containing synthetic organic dyes by electrochemical methods. An updated review, Appl. Catal. B Environ. 166 (2015) 603–643, https://doi.org/10.1016/j.apcatb.2014.11.016.

[35] A. Anglada, A. Urtiaga, I. Ortiz, Contributions of electrochemical oxidation to waste-water treatment: fundamentals and review of applications, J. Chem. Technol. Biotechnol. 84 (12) (2009) 1747–1755, https://doi.org/10.1002/jctb.2214.

[36] D. Knozowski, M. Gmurek, Non-active anodes based on boron-doped diamond, PbO2 and SnO2-Sb for anodic oxidation of water contaminants: synthesis, properties, and recent advances, Desalination Water Treat. 320 (2024), https://doi.org/10.1016/j.dwt.2024.100655.

[37] F. Liu, Z. Deng, D. Miao, W. Chen, Y. Wang, K. Zhou, L. Ma, Q. Wei, A highly stable microporous boron-doped diamond electrode etched by oxygen plasma for enhanced electrochemical ozone generation, J. Environ. Chem. Eng. 9 (6) (2021), https://doi.org/10.1016/j.jece.2021.106369.

[38] W. Zeng, H. Liang, H. Zhang, X. Luo, D. Lin, G. Li, Efficient electrochemical oxidation of sulfamethoxazole by a novel reduced TiO2 nanotube arrays-based flow-through electrocatalytic membrane, Separ. Purif. Technol. 289 (2022), https://doi.org/10.1016/j.seppur.2022.120720.

[39] J. Zhang, J. Ding, L. Liu, R. Wu, L. Ding, J. Jiang, J. Pang, Y. Li, N. Ren, S. Yang, Selective removal of sulfamethoxazole by a novel double Z-scheme photocatalyst: preferential recognition and degradation mechanism, Environ. Sci. Ecotechnol. 17 (2024), https://doi.org/10.1016/j.ese.2023.100308.

[40] Z. Su, L. Zhang, F. Jiang, M. Hong, Formation of crystalline TiO2 by anodic oxidation of titanium, progress. Natural. Sci. Mater. Intern 23 (3) (2013) 294–301, https://doi.org/10.1016/j.pnsc.2013.04.004.